Springer

Available online at https://link.springer.com/journal/42241
http://www.jhydrodynamics.com
Journal of Hydrodynamics, 2021, 33(1): 120-126
https://doi.org/10.1007/s42241-021-0007-y

Hydrodynamics of Euglena Gracilis during locomotion *

Fahrettin Gökhan Ergin
Product Management, Dantec Dynamics A/S, Skovlunde, Denmark

(Received September 24, 2020, Revised November 10, 2020, Accepted December 3, 2020, Published online February 24, 2021)

Abstract: The hydrodynamics and locomotion mechanism of Euglena Gracilis (*E. Gracilis*) is investigated using microscopic shadow imaging and micro particle image velocimetry (MicroPIV). Three distinct locomotion modes were observed: translation, spin, and left/right turn. Since the flagellum was not possible to image, the strokes were identified by evaluating the flow field around the protist. The flow field information is obtained using a phase-separated PIV evaluation, which uses a histogram-thresholding based dynamic masking approach. The temporal resolution of the experiment was sufficient to identify the sequence of two modes, translation and spin, and the stroke-pulling frequency. The flow field result during a stroke is compared with existing Stokeslet dipole theories and flow disturbance decay with distance is investigated. The results indicate that the organism has a complex locomotion technique that allows the change of direction, axial orientation and propulsion.

Key words: Euglena Gracilis (*E. Gracilis*) locomotion, micro particle image velocimetry (MicroPIV), dynamic masking

Introduction

Euglena Gracilis (*E. Gracilis*) is a protist microorganism that populates in freshwater habitats and sustains life by collecting solar energy by photosynthesis using chloroplasts. Its body length without the flagellum can vary between 20 μm and 100 μm. The optimum light level for chloroplasts is around 30 W/m^2, and therefore *E. Gracilis* is known to adjust its depth in water in order to find this optimum light condition[1]. This necessitates the photo detection, sense of gravity and locomotion, which are vital functionalities for *E. Gracilis*' survival. The basic aerotaxis (moving towards oxygen), gravitaxis (moving up and down) and phototaxis (moving towards or away from light) behavior is explained in detail in Ref. [1], where underlying chemistry necessary for locomotion is provided. In this section we provide a summary of *E. Gracilis* locomotion behavior from Ref. [1], which consists of thee modes forward translation, spin along long axis and the euglenoid movement. According to Ref. [1], the flagellum is actively used during translation and spin. In fact, *E. Gracilis* has two anterior trailing flagella, but only the long, protruding one is the main source of forward propulsion (Fig. 1(c)). The flagellum is located at one end close to the photoreceptor and the reservoir, whereas the cell nucleus is centrally located in its body. The flagellar beats could be in the form of pulling strokes that results in a forward translation, or rotational strokes that results in the *E. Gracilis* to spin around its long axis. In this work we are only interested in resolving the flagellar beats that are in the form of pulling strokes, i.e., stroke pulling frequency. The rotational movement of *E. Gracilis* is often associated with phototaxis, where the organism senses the light propagation direction[1]. This is accomplished by spin swimming where varying amplitudes of light is registered on the photoreceptor due to changing incidence angle of the light rays. This would normally create two maxima per spin, due to a dichroitic orientation of the photoreceptor molecules in the stigma (eye spot, Fig. 1(a)) the light direction is determined unambiguously. The final locomotion mode is the euglenoid movement, which can be described by the bending and stretching of the organism either in order to change direction or move forward like a snail. The euglenoid movement is often attributed to the pellicular stripes, microtubules that can slide on each other, which gives the extreme flexibility to *E. Gracilis*[1]. Recent SEM pictures of the *E. Gracilis* reveal that the pellicular stripes are oriented resembling the threads of a left-hand screw (Figs. 1(b), 1(c)), a schematic of which is given in Fig.

* **Biography:** Fahrettin Gökhan Ergin, Male, Ph. D., Product Manager
Corresponding author: Fahrettin Gökhan Ergin, E-mail: gokhan.ergin@dantecdynamics.com

1(d). The pellicular stripes are oriented at approximately 45° angle with respect to its long axis. This is determined by two separate image rotations applied on Fig. 1(c), first an 18° counterclockwise (CCW) rotation to align the long axis with the vertical, and second a 63° CCW rotation to align the stripes with the horizontal. The difference is the thread angle at the equatorial positions, which changes to 90° close to the anterior tip.

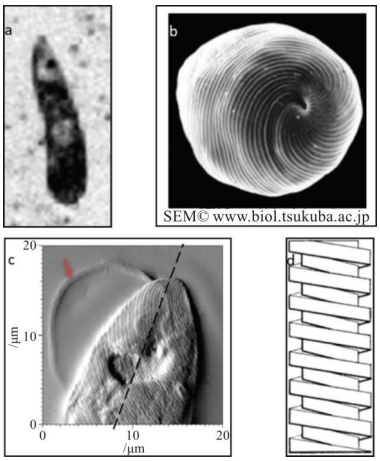

Fig. 1 (Color online) (a) Picture of the 48 µm-tall, 10 µm-diameter *E. Gracilis* under investigation (b) SEM image of the threaded screw like surface texture. Printed with permission. © Isao INOUYE, Institute of Biological Sciences, University of Tsukuba (c) AFM image of the threaded screw like surface texture. Image adapted from Fig. 4 in Ref. [2]. Reproduced with permission. Dashed line in (c) is the approximate location of the long axis and the red arrow marks the flagellum. (d) Schematic of a left-handed mechanical screw. Image credits: Wikipedia commons

Although much is known about *E. Gracilis*' locomotion behavior, a quantitative evaluation of hydrodynamics during locomotion has not been reported. In this study, the aim is to quantify these three modes (translation, spin and turns) using microscopic imaging, dynamic masking, and micro particle image velocimetry (MicroPIV). In the following sections the average linear swim speed, power required for swimming, hydrodynamics of the stroke mechanism, sequence of the swimming modes and the relation between threaded screw like surface texture and the spin mode are investigated.

1. Material and methods

1.1 *Experimental setup*

The experiments were performed in still water and a cold light source ensured that there was no background flow due to convection currents. The flow field around *E. Gracilis* is measured using time resolved MicroPIV. The use of particle imaging and tracking techniques for the investigation of flow fields of motile organisms is not new; some recent examples are given in Refs. [3]-[8]. The MicroPIV system is manufactured by Dantec Dynamics A/S (Skovlunde, Denmark), and is explained in detail in Ref. [9]. Briefly, the components include an inverted fluorescence Microscope, a sensitive CMOS detector, a synchronization device, and a pulsed LED illumination system. In biological flows, high-power pulsed laser illumination is not preferred as this can disable the organism. For this reason, a lower-power, green LED-based pulsed illumination was used in transmission mode. The green color simulates a natural environment, such as a freshwater pond surface where *E. Gracilis* flourish. 1 µm-diameter seeding particles were introduced in small quantities until a sufficient seeding density was achieved for PIV. The seeding density was kept at a low level to avoid possible changes in the normal swimming behavior. The particle images were recorded at a frame rate of 12.5 fps (constant time difference of 80 ms), at a resolution of 1 280 × 800 pixels. The images were acquired using a 40 × magnification objective, producing a 0.40 mm × 0.64 mm-wide field of view (FOV) and 1 µm-thick field depth. The small field depth ensures that the measured displacements are planar. Later a smaller region of interest is extracted with a resolution of 323 × 529 pixels, corresponding to 162 µm × 265 µm in the object space. Since the FOV was small (~0.25 mm^2), it was often necessary to wait until an organism swims through the FOV when the measurement system is in operation. The raw images were stored in a ring buffer and the acquisition is stopped manually after the organism passed through the FOV.

1.2 *Dynamic masking*

Before PIV evaluation, the image of *E. Gracilis* body was removed from the flow field using dynamic masking[9-11], and no effort was made to remove the flagellum. This is necessary because the movements of the organism are not related to the fluid motion in the vicinity of *E. Gracilis*. A good example is Fig. 3(a), where the fluid upstream of is pulled downwards as *E. Gracilis* is swimming upwards. If not removed, the moving features on *E. Gracilis* image (stigma, nucleus etc.) contributes to the cross-correlation function during the velocity calculation and introduces an error in of the flow field. The details of the image pre-processing steps used to achieve the dynamic mask are provided in Ref. [11]. Briefly, first a pixel inversion is performed to work with positive particle images instead of particle shadows. Second, a background subtraction is performed using the minimum pixel value found in the original ensemble.

Third, a histogram-thresholding based binary dynamic mask ensemble is produced using the images in the second step and finally image masking is performed by multiplication of the binary mask with the background-removed images. The dynamic mask captures the position and the shape of *E. Gracilis* in a successful fashion (Fig. 2).

Fig. 2 Position of *E. Gracilis* recorded every 0.96 s found by the dynamic mask

1.3 *Velocimetry*

Details of the velocity calculations are provided in Refs. [9, 11]. Briefly, an adaptive PIV algorithm is used, which is an advanced particle displacement estimator implemented in DynamicStudio (Dantec Dynamics, Skovlunde, Denmark). The calculation is a cross-correlation based, adaptive and iterative procedure with vector validation and deforming windows. For the current case, interrogation windows of 32×32 pixel are used with 75% overlap. Window deformation is performed by adapting the interrogation area shape to velocity gradients. Several passes can be made to further shift and deform the windows to minimize the in-plane particle dropout. This procedure is repeated until a convergence limit in pixels or a maximum number of iterations is reached. Then a 2-D Gaussian fit is performed on the highest correlation peak to calculate the displacement field with subpixel accuracy. Between passes, spurious vectors are identified and replaced with a number of validation schemes. The subpixel positioning accuracy of the Adaptive PIV algorithm is reported as 0.06 pixels with 95% confidence[12]. The 0.06 pixels correspond to a 27.5 nm displacement in the object space, and the velocity uncertainty is estimated at 0.34 μm/s. An average filter in a 5×5 neighborhood and vector masking are applied after Adaptive PIV computations.

2. Results

The swimming modes of the experiments are extracted from a single trajectory of a single organism performing 4 strokes and 4 spins where 2 right turns and 2 left turns were executed (Movie 1). In fact, each stroke is followed by a spin, which means the stroke-pulling frequency is equal to the spin frequency (Movie 1). *E. Gracilis* meanders upwards through filtered water, covering a net distance of approximately 256 μm and a gross displacement of 292 μm in 6.56 s, yielding an average swim speed of ~44.5 μm/s. The net to gross displacement ratio (NGDR) for this track is 0.88. The shape of the organism at equidistant time steps is shown in Fig. 2.

2.1 *Estimation of average linear drag force and average translation power*

The Reynolds number (Re) for this flow is 0.002 with an average linear swim speed of 44.5 μm/s and a characteristic length of 48 μm. Since the Re is $0.002 \ll 1$ we can safely assume Stoke's flow around the organism. The axial force on the organism, just for the forward translation motion, can be estimated using an analytical expression (Eq. (1)) developed for Stoke's flow on a prolate spheroid parallel to its long axis[13]:

$$F = 16\pi\mu Uae^3\left[(1+e^2)\lg\frac{1+e}{1-e} - 2e\right]^{-1},$$

$$e = \sqrt{1-\left(\frac{b}{a}\right)^2} \tag{1}$$

where μ is the dynamic viscosity (1.002 mPa·s), U is the axial swim velocity (44 μm/s), a is the half-length of the long axis (24 μm), and e is the eccentricity of the prolate spheroid (0.978). With values evaluated at 20°C, the estimated drag force on *E. Gracilis* is 25 pN, and the power required for swimming is estimated at 1.0 fW. For a better comparison with other motile cells of different sizes, the cost of propulsion per volume is more meaningful. The *E. Gracilis* under observation here has a volume of 2.5 fm^3, which results in a power to volume ratio of 0.4 W/m^3.

2.2 *Spin*

The first locomotion mode observed during the experiments is the spinning motion (Fig. 3). The motion can be observed by tracking the position of the stigma relative to the main axis. In Fig. 3(a), the stigma is located on the top right of the organism and moves towards the center and further to the left in time (Figs. 3(b)-3(f)). In time, the stigma becomes invisible as it moves below the organism (Movie 2). The swimmer is observed to spin in the same direction, counterclockwise looking from the trailing edge (Movie 1). There is a second motion in Fig. 3, which

can be observed by tracking the organism within the frame: the organism glides forward as it spins towards the left. This is important, as it resembles the motion of a left-handed mechanical screw. If a left-handed screw is turned left in a softer material it provides a forward translation motion along its long axis (left-hand grip rule).

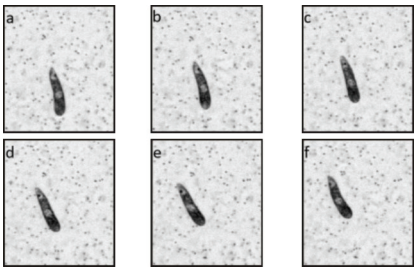

Fig. 3 Spinning motion of *E. Gracilis* at $t = 2.00$ s (a), $t = 2.16$ s (b), $t = 2.32$ s (c), $t = 2.48$ s (d), $t = 2.64$ s (e) and $t = 2.80$ s (f)

It is apparent that *E. Gracilis* has a rather steady spin speed, and it completes half a revolution in 0.8 s, and thus spin speed is 0.625 revs/s. The linear translation is computed by subtracting the tip position in Figs. 3(a), 3(f): *E. Gracilis* moves 32.65 μm forward in 0.8 s, resulting in a linear speed of 40.8 μm/s, and this is consistent with the average swim speed. When the linear and the rotational displacement per revolution of a screw (or a helical gear) are available, the helix angle and mechanical advantage can be calculated. The helix angle is defined as

$$\alpha = \tan^{-1}\left(\frac{l}{\pi D}\right) \tag{2}$$

where l is the lead (linear displacement), and D is the diameter (10 μm). The helix angle of an ideal mechanical screw with these properties would have been 64°. This value is larger than the helix angle 45° calculated using Fig. 1(c), which means the *E. Gracilis* achieves approximately twice the forward displacement of a mechanical screw. This difference can be explained by the forming shear layers present around *E. Gracilis* in water, which allows *E. Gracilis* to glide through the surrounding viscous medium.

2.3 *Stroke*

The flow field around *E. Gracilis* is measured using MicroPIV and dynamic masking. Close ups of the flow field during several stroke instances are shown in Fig. 4. In these figures, vectors represent the u and v components of the flow field and colors represent the magnitude of local velocity, where blue areas represent stagnant flow regions.

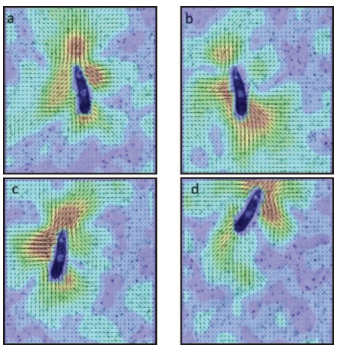

Fig. 4 (Color online) *E. Gracilis* pulling strokes at $t = 1.92$ s, 3.52 s, 4.32 s and 5.12 s

The stroking motion of the flagellum is distinguished by the inflow upstream of the *E. Gracilis* and towards the *E. Gracilis*. The stroke is observed first at $t = 1.92$ s, and then at $t = 3.52$ s, 4.32 s and 5.12 s, exactly every 0.80 s (corresponding to 1.25 Hz). The time difference between the 1.92 s and 3.52 s is 1.60 s, corresponding to half of 1.25 Hz. This is in very good agreement with the findings of Ref. [14] that report a cell body rotation frequency of 1.20 Hz for a single *E. Gracilis* using light scattering experiments (Fig. 3 in Ref. [14]). For a population of *E. Gracilis* the frequency band widens approximately 0.50 Hz (Fig. 4(a) in Ref. [14]). The term cell body rotation frequency used by Ref. [14] is an equivalent term to the spin frequency used in this work. The spin frequency is further equal to the stroke-pulling frequency as each stroke is followed by a spin (Movie 1). Furthermore, the Strouhal number based on this stroke-pulling frequency is calculated as 0.31, which is consistent with the literature for optimal swimming efficiency for oscillatory swimming[15] approximately 30.00 Hz for *E. Gracilis*[14, 16-18].

The flow field around *E. Gracilis* reveals that the fluid is drawn towards the organism upstream and downstream, and fluid is expelled from the organism on the sides (Fig. 4). The upstream flow field is produced by the flagellum pulling a stroke, the main source of propulsion. The downstream flow field can be explained as the wake in the aft of the swimmer. Due to continuity around the organism, the fluid is expelled outwards from the sides. This type of flow field produces four stagnant flow regions, one at each corner of the organism, i.e., due Southwest, Southeast, Northwest, and Northeast of the organism. These regions are more visible in Fig. 4(a). These findings are in very good agreement with two review articles on microscopic swimmers[19-20], both of which model the microscopic swimmers as Stokeslet dipoles, where the swimmer's body and propulsion appendage (in this case flagellum) is considered as two point masses

producing a drag force and a propulsive force on the surrounding fluid, respectively.

In order to demonstrate the similarities between the measured flow field around *E. Gracilis* (Fig. 5(a)) and the dipole Stokeslet theory, a three-way comparison can be made between Figs. 5(a)-5(c). Figure 5(b) shows a modified version of the schematic (Fig. 16(b)) reported in Ref. [19], and Fig. 5(c) shows the flow field calculated using Eq. 12 in Ref. [19] for a puller type swimmer travelling in the vertical direction (Eq. (3)) in a 150 μm×150 μm box with the dipole in the center. In Eq. (3), u_d is the dipole velocity field, r is the distance vector from the center of the force dipole, f_0 is the dipole force magnitude (1.25 fNm), d is the distance between the force pair with equal magnitude with opposite direction (50 μm), and η is the fluid dynamic viscosity (1.002 mPa·s).

$$u_d(\boldsymbol{r}) = \frac{f_0 d}{8\pi\eta r^3}\left[3\frac{(\boldsymbol{r}\cdot\hat{\boldsymbol{e}})^2}{r^2} - 1\right]\boldsymbol{r} \tag{3}$$

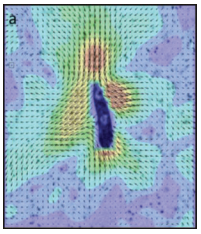

Fig. 5(a) (Color online) Measured flow field around *E. Gracilis* pulling a stroke at $t = 1.92$ s

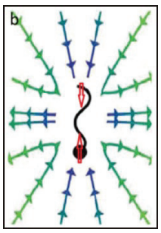

Fig. 5(b) (Color online) schematic of the flow field for a uni-flagellate "puller" type dipole swimmer

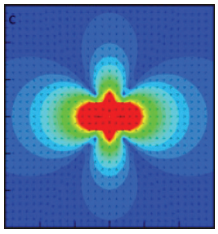

Fig. 5(c) (Color online) flow lines of an ideal hydrodynamic dipole puller-type swimmer in vertical direction using Eq. (3)

Apparent from the measurement results and confirmed by the calculated flow field, the flow disturbances produced by the organism extend well into the far field, especially upstream of the organism in the measurement results due to the flagellar activity. This is expected and is a result of viscosity-dominated flow in a low Reynolds number (Re) environment. According to Ref. [19] the flow disturbances decay in space with $\sim r^{-2}$. However, we observe that the disturbances in the flow field decay with $r^{*(-1.02)}$ (Fig. 6) for the measurement results and with $\sim r^{*(-2.25)}$ for the computational results (Fig. 5(c)). In Fig. 6, the normalized velocity disturbance $V^*(V/V_{\text{avg}})$ is plotted with respect to the normalized distance $r^*(r/L)$, where V_{avg} is the average swim speed, 44.5 μm and L is the length of *E. Gracilis*, 48 μm. The fitted curve is chosen as $V^* = ar^{*b}$ to find the exponent b that fits the data best. This indicates that the Stokeslet dipole equation (Eq. (2)) captures the general characteristics of the flow field produced by a puller-type swimmer such as flow topology and direction but is not sufficient to estimate the decay of the actual flow disturbances, i.e., with $\sim 1/r^*$. It should be noted that the R^2 value for the fit is only around 0.4 due to scatter in the data points for $r^* < 1$. Another observation is that the small flow disturbances reach up to around 3 times the length of *E. Gracilis*, whereas the larger disturbances reach only within 1 length.

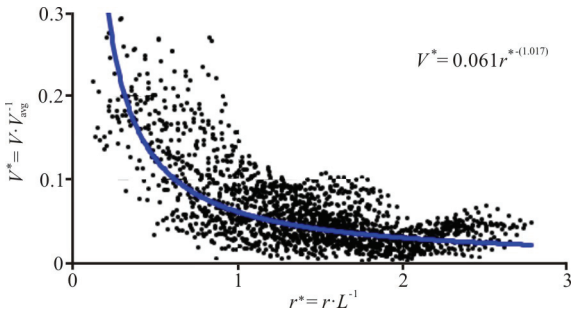

Fig. 6 (Color online) Decay of flow disturbances produced by *E. Gracilis* pulling a stroke at $t = 1.92$ s (Fig. 5(a)). Blue curve is the fit performed on the data points using $V^* = ar^{*b}$

2.4 *Sequence of locomotion modes: Stroke and spin*

Once the two major swimming modes are established, it is interesting to know the sequence of events: in other words, whether the stroke and spin are simultaneous or whether one is after the other.

Figure 7 shows the flow field around *E. Gracilis* during a stroke followed by a spin where flow fields

are shown with equal time spacing of 240 ms. In Fig. 7(a), *E. Gracilis* is at the beginning of pulling a stroke, where the fluid upstream of *E. Gracilis* has just started moving towards the organism. In Fig. 7(b), the stroke is close to its maximum power where the pulled (upstream) and expelled (on each side) fluid velocities reach to maximum values. In Fig. 7(c), the stroke is slowing down and comes to an end in Fig. 7(d), when *E. Gracilis* starts its spin as the stigma begins moving towards the left. The spinning motion continues in Fig. 7(e), 7(f). Since the flagellum is not visible in the raw images it is not possible to clarify whether *E. Gracilis* actively rotates the flagellum in the clockwise (CW) direction in order to spin in the ccw direction, or it just passively lets the fluid friction along the pellicular stripes put itself in a spiral motion.

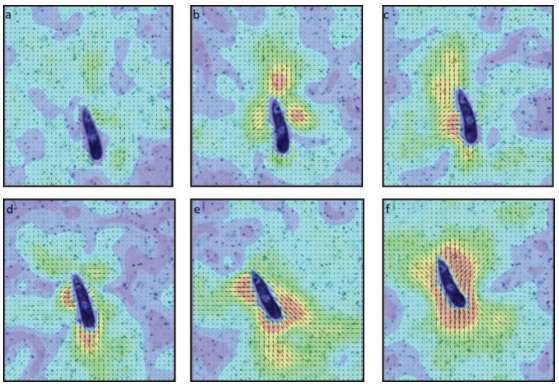

Fig. 7 (Color online) *E. Gracilis* during a stroke at t = 1.6 s, 1.84 s and 2.08 s followed by a spin at t = 2.32 s, 2.56 s and 2.80 s

2.5 *Left and right turns*

During the experiments *E. Gracilis* executes two left turns (these are shown in Figs. 8(a), 8(b)) and two right turns (these are shown in Figs. 8(c), 8(d)). An important observation is made from the hydrodynamics of the flow field during turns: when *E. Gracilis* is turning left, it creates vortex on its left (Figs. 8(a), 8(b)), and when it is turning right, it creates a vortex on its right (Figs. 8(c), 8(d)). The vortex core is located closer to the trailing edge of *E. Gracilis* at a distance of 1 to 3 diameters from the organism.

The creation of these vortices can be explained by the local pressure distribution around *E. Gracilis.* First, since *E. Gracilis* is in forward motion, there is normally a constant suction pressure on its tail. During a left turn, the fluid on the left is being pushed leftwards, and therefore a positive pressure on the left is formed (Figs. 8(a), 8(b)). The continuity equation must be satisfied in this viscous flow and the fluid under suction pressure in the wake of *E. Gracilis* is replaced by the fluid under positive pressure on its left. This forces the fluid to rotate and form a CCW vortex on the left. The opposite happens during a right turn, a positive pressure is formed on the right-hand side and this fluid replaces the fluid in the wake. This forces the fluid to rotate and form a CW vortex on the right. Due to the presence of a vortex during turns, the flow disturbances created during turns can extend up to 5 to 6 diameters from the organism which increases the risk of detection by predators. It is not yet clear how the *E. Gracilis* mechanically initiates each turn, but there are three possibilities: (1) bending its body in the direction of the turn (Figs. 8(a), 8(c) and 8(d)), (2) using the flagellum in a complex stroke or (3) a combination of these two. It was suggested that uni-flagellate bacteria with posterior-attached flagella ("fluid pushers") exploit a buckling instability of the hook to change direction during forward swimming[21]. It is not clear whether a similar mechanism is involved here since the forward swim is achieved by pulling strokes in the case of *E. Gracilis*, where the flagellum is attached in the anterior.

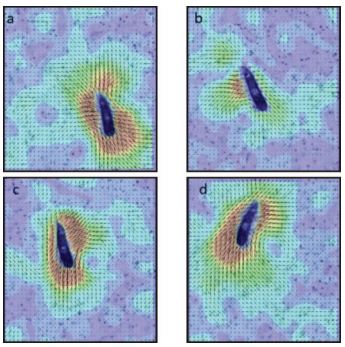

Fig. 8 (Color online) *E. Gracilis* performing left turns ((a), (b)) and right turns ((c), (d))

3. Discussion

The quantitative experimental results provide significant insight into *E. Gracilis* locomotion hydrodynamics. First and foremost, the sequence of spin and stroke mechanisms is established. It is interesting that the *E. Gracilis* pulls a stroke followed by a spin, which is similar to the human freestyle swim technique. How the organism initiates the spin is still not very clear; passively due to helical pellicular stripes, actively using the flagellum or a combination of both. Second, the angular orientation and handedness (twist direction) of the pellicular stripes is established. There are sufficient reasons to think that the left-handed helical pellicular stripes either assist or sustain the spinning motion of *E. Gracilis*. Third, the average spin speed, average swim speed, linear drag force and swim power are calculated. The average swim power is related to the average power used in the flagellum during strokes for forward translation only. This is a first step for estimating the locomotion

cost for *E. Gracilis* in search for nutrient zones in darkness, move towards light in low light conditions or move away from light in excessive light conditions. This information can be used in estimating the minimum amount of nutrients required to keep an *E. Gracilis* culture alive and moving during extended periods of darkness, for example during space travel. Fourth, the hydrodynamics related to stroke and left / right turns are established. The results indicate that during stroke and turns the hydrodynamic flow disturbances can reach as much as 5-7 diameters, and this increases the risk of detection by predators. Additionally, vortical structures are introduced in the flow during strokes and turns, which enhance mixing in the vicinity of *E. Gracilis*. As mentioned above, there are a number of unanswered questions that can be resolved by imaging the flagellum during micro-PIV experiments: (1) whether flagellum plays an active role during spin initiation, (2) higher-frequency flagellar beating frequency, and (3) how the flagellum is used during turns. Future work aims to utilize a fluorescence-staining technique reported in Ref. [22] in the real-time imaging of the flagellum during MicroPIV experiments. Since the flagellum can rotate in three dimensions, future experiments are planned to measure the third velocity component using a high-speed stereoscopic PIV system in a plane or a volumetric system in the entire volume.

Acknowledgement

The author wishes to thank Giovanni Noselli for providing the culture for Euglena Gracilis, and Lalith Wickramarathna for many helpful comments and suggestions.

References

[1] Häder D. P., Faddoul J., Lebert M. et al. Investigation of gravitaxis and phototaxis in Euglena Gracilis (Sinha A. K. R. R. P., Sharma N. K. Advances in life sciences) [M]. New Delhi, India: I. K. International Publishing House Pvt. Ltd., 2010, 117-131.

[2] Gruenberger C., Ritter R., Aumayr F. et al. Algal biophysics: Euglena Gracilis investigated by atomic force microscopy [J]. *Materials Science Forum*, 2007, 555: 411-416.

[3] Nielsen L. T., Kiørboe T. Feeding currents facilitate a mixotrophic way of life [J]. *ISME Journal*, 2015, 9(10): 2117-2127.

[4] Kiorboe T., Jiang H., Goncalves R. J. et al. Flow disturbances generated by feeding and swimming zooplankton [J]. *Proceedings of the National Academy of Sciences of the United States of America*, 2014, 111(32): 11738-11743.

[5] Wadhwa N., Anderse A., Kiorboe T. Hydrodynamics and energetics of jumping copepod nauplii and copepodids [J]. *Journal of Experimental Biology*, 2014, 217(17): 3085-3094.

[6] Rope M., Dayel M. J., Pepper R. E. et al. Cooperatively generated stresslet flows supply fresh fluid to multicellular choanoflagellate colonies [J]. *Physical Review Letters*, 2013, 110(22): 228104.

[7] Pepper R. E., Roper M., Ryu S. et al. Nearby boundaries create eddies near microscopic filter feeders [J]. *Journal of the Royal Society Interface*, 2010, 7(46): 851-862.

[8] Guasto J. S., Johnson K. A., Gollub J. P. Oscillatory flows induced by microorganisms swimming in two dimensions [J]. *Physical Review Letters*, 2010, 105(16): 168102.

[9] Ergin F. G. Flow field measurements during microorganism locomotion using MicroPIV and dynamic masking [C]. *11th International Symposium on Particle Image Velocimetry*, Santa Barbara, California, USA, 2015.

[10] Ergin F. G. On dynamic masking of time resolved PIV data [C]. *10th European Fluid Mechanics Conference (EUROMECH)*, Copenhagen, Demark, 2014.

[11] Ergin F. G. Dynamic masking techniques for particle image velocimetry [J]. *Journal of Thermal Sciences and Technology*, 2017, 37(2): 61-74.

[12] Ergin F. G., Watz B. B., Erglis K. et al. Time-resolved velocity measurements in a magnetic micromixer [J]. *Experimental Thermal and Fluid Science*, 2015, 67: 6-13.

[13] Srivastava D., Yadav R., Yadav S. Steady Oseen flow past deformed sphere: An analytic approach [J]. *Journal of Teoretical and Applied Mechanics*, 2013, 51(3): 661-673.

[14] Angelini F., Ascoli C., Frediani C. et al. Transient photoresponses of a phototactic microorganism, haematococcus pluvialis, revealed by light scattering [J]. *Biophysical Journal*, 1986, 50(5): 929-936.

[15] Triantafyllou G. S., Triantafyllou M. S., Grosenbaugh M. A. Optimal thrust development in oscillating foils with application to fish propulsion [J]. *Journal of Fluids and Structures*, 1993, 7(2): 205-224.

[16] Ascoli C., Barbi M., Frediani C. et al. Measurements of Euglena motion parameters by laser light scattering [J]. *Biophysical Journal*, 1978, 24(3): 585-599.

[17] Ascoli C., Frediani C. Quasi-elastic light scattering in the measurement of the motion of flagellated algae (Light scattering in liquids and macromolecular solutions) [M]. Boston, MA, USA: Springer, 1980, 183-198.

[18] Chen S. H., Hallett F. R. Determination of motile behaviour of prokaryotic and eukaryotic cells by quasi-elastic light scattering [J]. *Quarterly Reviews of Biophysics*, 1982, 15(1): 131-222.

[19] Elgeti J., Winkler R. G., Gompper G. Physics of microswimmers−single particle motion and collective behavior: A review [J]. *Reports on Progress in Physics*, 2015, 78(5): 056601.

[20] Lauga E., Powers T. R. The hydrodynamics of swimming microorganisms [J]. *Reports on Progress in Physics*, 2009, 72(9): 096601.

[21] Son K., Guasto J. S., Stocker R. Bacteria can exploit a flagellar buckling instability to change direction [J]. *Nature Physics*, 2013, 9(8): 494-498.

[22] Turner L., Ryu W. S., Berg H. C. Real-time imaging of fluorescent flagellar filaments [J]. *Journal of Bacteriology*, 2000, 182(10): 2793-2801.